https://doi.org/10.5194/os-2019-93
Preprint. Discussion started: 5 August 2019

Ocean Science
Discussions
Open Access
EGU

Influence of intraseasonal eastern boundary circulation variability on hydrography and biogeochemistry off Peru

Jan Lüdke[1], Marcus Dengler[1], Stefan Sommer[1], David Clemens[1], Sören Thomsen[2], Gerd Krahmann[1], Andrew W. Dale[1], Eric P. Achterberg[1,3], Martin Visbeck[1,3]

[1]GEOMAR Helmholtz Centre for Ocean Research Kiel, Düsternbrooker Weg 20, D-24105 Kiel, Germany

[2]LOCEAN-IPSL, IRD/CNRS/Sorbonnes Universites (UPMC)/MNHN, UMR 7159, Paris, France

[3]Kiel University, Kiel, Germany

Correspondence to: Jan Lüdke (jluedke@geomar.de)

Abstract. The Peruvian Upwelling System is characterized by high primary productivity fuelled by the supply of nutrients in a highly dynamic boundary circulation. The intraseasonal evolution of the physical and biogeochemical properties is analysed based on shipboard observations and remote sensing conducted between April and June 2017 off central Peru. The poleward transport in the subsurface Peru Chile Undercurrent was highly variable and strongly intensified between mid and end of May. This intensification was likely caused by a first baroclinic mode downwelling coastal trapped wave excited at the equator at about 95°W that propagated poleward along the South American coast. The intensified poleward flow shortens the time of water mass advection from the equatorial current system to the study site. The impact of the anomalous advection is mostly noticed in the nitrogen cycle because during the shorter time needed for poleward advection less fixed nitrogen loss occurs within the waters. This causes a strong increase of nitrate concentrations and a decrease in the nitrogen deficit. These changes suggest that the advection caused by the coastal trapped wave supersedes the simultaneous effect of anomalous downwelling in terms of nutrient response.

1 Introduction

The eastern boundary circulation off Peru is dominated by wind driven upwelling near the surface and the poleward Peru-Chile Undercurrent (PCUC) occupying the upper slope and shelf at depths of about 50 to 200 m (Fig. 1, e.g. Gunter, 1936; Chaigneau et al., 2013). Mean poleward velocities associated with the PCUC are between 0.05 and 0.15 ms^{-1} (Chaigneau et al., 2013). The origin of its source waters is still under debate. Chaigneau et al. (2013) back-traced its origin to the Equatorial Undercurrent via the Ecuador-Peru Coastal Current flowing southward along the coast between the equator and 5 °S. In contrast, a regional model analysis by Montes et al. (2010) suggests that the source waters of the PCUC originate predominately from the eastward Southern Subsurface Countercurrents south of the equator (Fig. 1). Upwelling dynamics

https://doi.org/10.5194/os-2019-93
Preprint. Discussion started: 5 August 2019

imply the existence of an equatorward geostrophic surface jet above the PCUC, the Peru Coastal Current (e.g. Hill et al.., 1998; Kämpf and Chapman, 2016) as evidenced by model simulations (Montes et al., 2010). Additionally, observational and modelling studies suggest equatorward flow offshore (Peru-Chile Current) and below (Chile-Peru Deep Coastal Current) the PCUC as well (Fig. 1, Strub et al., 1998; Penven et al., 2005; Czeschel et al., 2011; Chaigneau et al., 2013).

In the Peruvian Upwelling System (PUS) low oxygen, high nutrient Equatorial Subsurface Waters (ESSW) transported poleward by the PCUC upwells (Brink at al., 1983; Penven et al., 2005; Silva et al., 2009; Albert et al., 2010; Chaigneau et al., 2013; Grados et al., 2018). The PUS in the eastern tropical south Pacific (ETSP) is among the most productive regions in the world ocean resulting in economically important fish catches (e.g. Carr, 2002; Chavez et al., 2008). Equatorward winds favour upwelling throughout the entire year (Bakun and Nelson, 1991; Strub et al., 1998) and enable a supply of nutrients from the subsurface water to the euphotic zone feeding the high primary productivity (Pennington et al., 2006).

Beneath the upwelling system, the low oxygen waters supplied to the PUS and enhanced local oxygen consumption due to remineralization of exported organic matter lead to the development of a pronounced oxygen minimum zone (OMZ) and anoxic conditions between about 30-70 m and 400-500 m depth (e.g. Karstensen et al., 2008; Revsbech et al., 2009; Brandt et al., 2015; Thomsen at al. 2016). In anoxic waters, the microbial mediated processes of denitrification and anammox convert bioavailable dissolved inorganic nitrogen (N), i.e. nitrate, nitrite and ammonium to nitrogen gas (N_2) and nitrous oxide (N_2O) which are subsequently outgassed to the atmosphere. N_2 fixation by diazotrophic organisms counteracts this loss of N-nutrients (N-loss). It is still a matter of debate whether the global ocean N cycle is presently in balance (e.g. Gruber, 2004; DeVries et al., 2013). An imbalance of the N fluxes with more (less) N-loss than N_2 fixation would reduce (enhance) future primary productivity and thus reduce (enhance) the capacity of phytoplankton to sequester CO_2 in the ocean (e.g. Codispoti, 2007).

The PUS exhibits variability on a wide range of time scales including intraseasonal (e.g. Brink et al., 1982; Belmadani et al., 2012; Pietri et al., 2014, Illig et al., 2018a, 2018b), seasonal (e.g. Pizarro et al., 2002; Chaigneau et al., 2013), and interannual to decadal (Pizarro et al., 2002; Ramos et al., 2008). Intraseasonal variability is either forced locally by changes of the wind stress and its curl (e.g. McCreary and Chao, 1985; Klenz et al., 2019) or remotely with subsequent propagation of the variability in the form of coastal trapped waves (CTW) (e.g. Brink, 1982).

Often, intraseasonal variability in the PUS is of equatorial origin and propagates poleward along the continental slope in the form of a CTW. Wind events in the equatorial Pacific can generate equatorial Kelvin waves that propagate eastward and upon reaching the continental margin are reflected into CTWs moving poleward along the shelf break (e.g. Enfield et al., 1987; Rydbeck at al., 2019). The poleward propagating CTWs modulate the velocities of the alongshore circulation (Shaffer et al., 1997; Pizarro et al.; 2002; Pietri et al., 2014), and thereby change the horizontal and vertical supply of nutrients. This affects the nutrient concentrations (Graco et al., 2017), benthic ecosystems (Gutierrez et al., 2008) and the productivity of the upwelling system (Echevin et al., 2014). CTW-induced changes in upwelling also contribute to sea surface temperature (SST) variability (Dewitte et al., 2011; Illig et al., 2014) along the South American coast. The influence of remote equatorial

https://doi.org/10.5194/os-2019-93
Preprint. Discussion started: 5 August 2019

signals by CTWs extends poleward to the Chilean margin to about 30 °S (Shaffer et al., 1997; Hormazabal et al., 2002; Illig et al., 2018b).

Here, we analyse the impact of an individual CTW observed during several field campaigns in austral autumn 2017 off Peru near 12°S spanning a period of more than two months. By repeating stations several times we provide a time series that allows us to distinguish the intraseasonal variability from that of shorter time scales due to local processes. The required high temporal resolution is missing in long term time-series data based on monthly or longer scales such as used by Graco et al. (2017) to analyse the interannual variability. Previous studies of the intraseasonal variability are based on modelling (e.g. Echevin et al., 2014) or restricted to circulation (e.g Pietri et al., 2014) or surface variables only (e.g. observations used by Dewitte et al. (2011) and Illig et al. (2014)).

The conditions off Peru in early 2017 were further affected by anomalously warm temperatures in the upper ocean during March associated with a coastal El Niño event (e.g. Garreaud, 2018; Echevin et al., 2018). Our observations on which this analysis is based cover the declining phase of the coastal El Niño event in April and May when SST anomalies were decreasing.

2 Data

2.1 Ship data

Within the framework of the Collaborative Research Center 754 “Climate-biogeochemistry interactions in the tropical ocean” R/V Meteor carried out a combined physical and biogeochemical sampling program in the ETSP off Peru from April to June 2017 (Tab. 1). A regional focus during the 4 individual cruises of the sampling program was a transect starting at shallow waters off Callao (Peru) at about 12 °S running offshore perpendicular to the coastline to water depth larger than 5000 m more than 100 km offshore (Fig. 1). In the following, this transect will be called the 12°S section. During the first cruise of R/V Meteor (Tab. 1) the 12 °S section was occupied at the end of the cruise on April 7 - 8. The two subsequent cruises focused on benthic and pelagic work along the 12 °S section. Time consuming benthic lander measurements (e.g. Sommer et al., 2016) required the vessel to remain close to the 12 °S section between April 18 and May 29, 2017, when repeated hydrographic and velocity measurements along the section were collected. The 12 °S section was again resampled during the final cruise M138 on June 24. In this study, we analyse shipboard velocity data collected by ocean surveyors, hydrographic profiles from the repeat measurements at 12 °S as well as oxygen and nutrient concentration measurements that were determined from water samples and optical sensors.

2.1.1 Shipboard velocity observations

During the cruises upper ocean velocities were recorded continuously using the vessel mounted ADCP systems (vmADCP) of R/V Meteor. One Ocean Surveyor vmADCP was operating with a frequency of 75 kHZ (OS75). During different phases of the cruises, the OS75 was recording velocity at bins of 4, 8 or 16 m depth, depending on the availability of backscattering

https://doi.org/10.5194/os-2019-93
Preprint. Discussion started: 5 August 2019

signals and the focus of investigation. The second vmADCP operated at 38 kHz (OS38) and recorded 32 bins covering a larger depth range than the OS75. During post-processing, vmADCP velocities were corrected using a mean amplitude and misalignment angle determined by a water-track calibration (e.g. Fischer et al., 2003). Misalignment angles from individual ship accelerations and turns followed a Gaussian distribution having a standard deviation of 0.65° for the OS75 and 0.75° for the OS38 (Sommer et al., 2019). A temporal trend was not detectable. The resulting error of the mean misalignment determined from more than 100 stations is thus less than 0.1°. An erroneous misalignment correction hinders the complete removal of the ship velocity from the observed velocities. Here, the magnitude of the velocity bias of our data due to uncertainties in the alignment angle calibration is below 1 cm s^{-1}. Fischer et al. (2003) considered an accuracy of 3 cm s^{-1} for 16 m bins in the upper 600 m under calm conditions in the tropics.

2.1.2 Hydrographic observations

At the 12 °S section a total of 151 hydrographic profiles were collected during the cruises M136 and M137 with a lowered SeaBird SBE 9-plus conductivity-temperature-depth (CTD) system using two pumped oxygen, temperature and conductivity sensors each. The CTD was attached to a General Oceanics rosette with 24 Niskin bottles of 10 l each to collect water samples. For the calibration of the conductivity sensor water samples were analysed with a Guildline Autosal Salinometer model 8400 B. The salinity calibration was done using a linear fit with respect to temperature, pressure and conductivity of CTD measurements to the salinometer measurements. Oxygen calibration was performed using Winkler titration of water samples (Winkler, 1888; Grasshoff et al., 1983). Processing and calibration followed the GO-SHIP recommendations (Hood et al., 2010). Correction coefficients for the CTD's conductivity sensors were derived using a multiparameter fit of the Autosal conductivities against the uncalibrated CTD sensor measurements. Coefficients included an offset and factors for temperature, pressure and conductivity.

From previous studies using STOX (Switchable Trace amount Oxygen) sensors, the OMZ off Peru is known to be anoxic and in its core the oxygen concentrations are below the detection limit of the Winkler titration method (Revsbech et al., 2009; Thomsen et al., 2016). From all water samples collected within the supposedly anoxic zone a mean oxygen concentration offset was calculated (2.26 µmol l^{-1}) and subtracted. As we assume this offset to stem from oxygen entering the water sample during the sampling process, the subtracted offset was scaled by the relative apparent oxygen utilization (AOU). Calibration coefficients were derived using a multiparameter fit of corrected Winkler oxygen concentrations against uncalibrated CTD sensor measurements. Coefficients were derived for offset, pressure and pressure squared, temperature, oxygen and oxygen squared, as well as for the product of oxygen and pressure.

Calibration of the salinity and oxygen sensors was performed separately for each cruise, except for M136 where the mean of the calibration of the preceding and succeeding cruises M135 and M137 was used (M136 lacked the required deep water samples). The final post-cruise calibration of the data resulted in an accuracy for temperature, salinity, and oxygen of 0.002 °C, 0.002 g kg^{-1} and 1.5 µmol kg^{-1}, respectively.

https://doi.org/10.5194/os-2019-93
Preprint. Discussion started: 5 August 2019

2.1.3 Nutrient measurements

Water samples collected on the upcast of the CTD rosette were used to determine nutrient concentrations. Concentrations of nitrate, nitrite and phosphate were measured using a QuAAtro autoanalyzer (Seal Analytical) with the precision of 0.1 µmol l^{-1}, 0.1 µmol l^{-1}, and 0.2 µmol l^{-1}, respectively (Sommer et al., 2019). Ammonium concentrations were measured using a fluorimetric methodology according to Holmes et al. (1999).

In addition to analysed water samples, concentrations of nitrate were measured using a Satlantic Deep Submersible Ultraviolet Nitrate Analyzer (SUNA) mounted on the CTD rosette. SUNA measurements are based on the absorbance spectra of ultraviolet light (Sakamoto et al., 2009). Data post-processing followed Karstensen et al. (2017) and Thomsen et al. (2019). Finally, the SUNA nitrate concentrations were calibrated against the nitrate measurements by the autoanalyzer using a linear fit.

2.2 Additional data

In addition to the cruise data we used sea level anomaly (SLA) based on satellite altimeter measurements that were provided by the E.U. Copernicus Marine Environmental Monitoring Service (product: SEALEVEL_GLO_PHY_L4_REP_OBSERVATIONS_008_047). This is a level 4 dataset derived by merging all available satellite altimetry data into one gridded product. Reprocessed data from January 1, 1993 to January 1, 2018 with the release days January 15, 2018 (data before May 15, 2017) and May 16, 2018 was used.

3 Methods

3.1 Analysis of velocity observations

The continuous velocity recording was split into segments when the ship was moving in on- or offshore directions only. The velocities were rotated to derive the alongshore component and then a mean velocity section was calculated for each segment of the cruise in 2 km bins according to offshore distance. Periods where the ship was moving slower than 1 kn were excluded, to restrict the analysis on periods where the ship was steaming. To derive the sections of alongshore velocity over longer time periods, the data from several of these segments were averaged. The presented sections were smoothed using a 2D Gaussian weighting with an influence radius of 4 km (8 m) and a cut-off of 6 km (18 m) horizontally (vertically).

3.2 Analysis of hydrographic and biogeochemical data

The analysis of hydrographic data is based on the TEOS10 definitions (IOC et al, 2010) and conservative temperature, absolute salinity and (potential) density were calculated with the Matlab Gibbs Seawater Toolbox (McDougall and Barker, 2011; Version 3.05)

https://doi.org/10.5194/os-2019-93
Preprint. Discussion started: 5 August 2019

3.2.1 Nitrogen deficit

To analyse the importance of N-loss processes in waters off Peru during the advection to the 12 °S section, we determined the nitrogen deficit. A deficit or excess in nitrogen exists if the ratio of nitrogen to phosphorus deviates from a ratio occurring during the assimilation and remineralisation of organic matter (Redfield ratio), especially if N-loss or N_2 fixation is prevalent in the water mass (Gruber and Sarmiento, 1997). We apply an empirical formula of nitrogen deficit by Chang et al. (2010) which bases the deficit on the deviation from the ratio between nitrogen species and phosphate measured outside of the eastern tropical south Pacific OMZ. The nitrogen deficit is calculated as:

$$N_{def} = 15.8\ (PO_4^{3-} - 0.3) - (NO_3^- + NO_2^- + NH_4^+) \quad (1)$$

Where PO_4^{3-}, NO_3^-, NO_2^-, and NH_4^+ are the concentrations of phosphate, nitrate, nitrite and ammonium. With this definition, positive values of N_{def} quantify the N-loss that has occurred within a certain water mass within the Peruvian OMZ.

3.2.2 Section averaging

Hydrographic and biogeochemical properties along the 12°S section analysed in this study have been calculated by first interpolating the data onto common potential density surfaces. Performing the further analysis in density space removes the effect of internal waves which can cause strong up- or downward displacements of properties in the water column. The profiles have been averaged in bins of 2 km according to distance from the coastline in density space, this was done to include frequently sampled stations only once in the sections. Averaging over several profiles at the same station allows reducing the impact on the result of variability on shorter time scales than the averaging period. The data was smoothed using a 2D Gaussian weighting with a density influence range of 0.03 kg m^{-3} and a cut-off range of 0.05 kg m^{-3} and respectively an influence and cut-off range of 3 and 6 km within 40 km of the coast, 7 and 15 km within 80 km and 15 and 20 km for more than 80 km offshore. The decreasing scale of horizontal interpolation towards the coast was used to benefit from the increased number of profiles to display smaller scale features. Finally, the fields were interpolated onto the mean section of potential density calculated in depth space.

3.3 Sea level anomaly data

The SLA along the 12°S section was calculated by averaging all daily data points of gridded SLA between 12 and 12.5 °S over the time periods used for the velocity sections and interpolating them onto the section according to the distance to the coast. Grid points closer than 30 km to the coast have been excluded. The mean SLA along the section was subtracted in order to restrict it on the on-offshore gradient.

To analyse intraseasonal variability along the equator and coastline at each grid point the mean SLA over the 25 year time series was subtracted before bandpass filtering using a 4th order Butterworth filter for a time window between 20 and 90 days. The wave track along the equator and the South American coast was calculated by averaging the bandpass filtered SLA

https://doi.org/10.5194/os-2019-93
Preprint. Discussion started: 5 August 2019

between 0.25 °S and 0.25°N (equivalent to 2 grid points) along the equator and by averaging the two grid points closest to the coast for the coastal wave track.

3.4 Theoretical coastal trapped wave structure

To interpret the observed flow variability along the Peruvian coast in terms of CTW, the cross-shore-depth structure of CTWs was determined by considering the linear, hydrostatic, inviscid, and Boussinesq approximated equations of motion on an f-plane using local bathymetry and stratification (Brink, 1982; 1989; Illig et al., 2018a). For alongshore scales larger than cross-shore scales and horizontally uniform stratification, cross-shore-vertical mode structures (eigenfunctions) and corresponding phase velocities (eigenvalues) solutions can be obtained from the simplified set of equations by using a resonance iteration approach (Brink, 1982; Brink and Chapman, 1987).

Here, we obtained the eigenfunctions and eigenvalues for the first three modes by applying a modified version of the Brink and Chapman (1987) Coastal-Trapped Wave programs as published by Brink (2018). These solutions have been used successfully in previous analyses of CTW structures in observational and model data (e.g. Brink et al., 1982; Pietri et al., 2014; Illig et al., 2018a).

The topography was taken from the data collected during the cruises, a mean depth was calculated in 5 km bins according to distance from the coast, resulting in a monotonic increase of water depth. Below 5000 m the depth was set to constant. The onshore closed boundary was set 10 km from the coast, effectively shifting the coordinate system, and with the depth measured 10 km off the coast.

From two offshore CTD profiles (M136 #60 and M137 #92) exceeding 3000 m depth a stratification profile was calculated first for each profile using 20 data points with 1 dbar spacing and then a mean profile was calculated from both casts in 5 m intervals.

4 Results

4.1 Variability of the boundary circulation

We observed the alongshore circulation at the 12 °S section for a period of more than eleven weeks by direct shipboard velocity measurements of the OS75 vmADCP (Fig. 2). From early April to June 24, 2017, the eastern boundary circulation was highly variable. However, in the upper 100m and inshore of 40 km, flow was consistently poleward.

In early April, the PCUC extended 80 km offshore (Fig. 2(a)) but then decreased in strength until mid-April when poleward flow was present only on the shelf (Fig. 2(b)). The initially weak increase (1 cm over 40 km) of sea surface height anomaly towards the coast (Fig. 2(a)) vanished during this period as well (Fig. 2(b) and (c)). At the end of April, the PCUC started to increase in strength, extended further offshore and to greater depth. About 14 days later in mid-May, the PCUC had strengthened considerably and its core reached maximum velocities of about 50 cm s^{-1} between 50 and 100 m depth 50 km offshore (Fig. 2(e)). During this time period, poleward flow extended more than 80 km offshore and occupied the water

https://doi.org/10.5194/os-2019-93
Preprint. Discussion started: 5 August 2019

column above 400 m depth. Sea surface height anomaly increased towards the coast (by 2 cm over 40 km) implying that a poleward geostrophic velocity anomaly was present at the sea surface as well. Towards the end of May, PCUC core velocities slightly decreased but remained above 40 cm s^{-1}. No data are available from the first three weeks of June. However, during the final section occupation on June 24, the PCUC had weakened drastically and maximum poleward velocities were only 10 cm s^{-1} (Fig. 2(g)).

In April, the velocity sections indicated equatorward flow offshore and below the PCUC (Fig. 2). In these depth and offshore ranges, the Peru Coastal Current and the Chile-Peru Deep Coastal Current are thought to be located (e.g. Penven et al., 2005). When the PCUC weakened in late April, the equatorward flow increased in strength and extended to shallower depth (Fig. 2(b) and (c)). However, during the period of strong poleward flow in May, the equatorward flow decreased and was present only below 400 m depth close to the offshore end of the section (Fig. 2(e) and (f)). On June 24, weak equatorward flow was present below 200 m at most parts of the section but never reached velocities of 10 cm s^{-1}. We found no indication of equatorward flow above or inshore of the PCUC, where the equatorward surface jet is expected to be situated.

To compare the alongshore circulation with hydrographic and biogeochemical sampling, the data was averaged into two periods: The initial phase of weak poleward flow (Fig. 3(a)) covering the period from April 18 – May 3, and a period of elevated poleward flow 12-29 May (Fig. 3(b)).

4.2 Coastal trapped wave characteristics

Coastal trapped waves are a known mechanism to intensify the velocity of the alongshore circulation. To determine if the changes of the circulation can be attributed to a CTW we compare the observed velocity structure to the cross-shore-depth structure of the first 3 CTW modes (see section 3.4) and discuss SLA along the coast for coherent propagating signals.

The cross-shore-depth structure of velocity obtained for the first three CTW modes at the 12° section varies predominately in the vertical axis with poles of opposing velocity located above each other (Fig. 4). Flow reversal for each individual mode occurs at shallower depth away from the boundary compared to inshore regions. As expected, higher modes exhibit an upper pole of enhanced velocity at shallower depth compared to lower modes.

For comparison, we show full-depth OS38 vmADCP alongshore velocities averaged over the period of the strong PCUC in the upper ocean (May 12 – 29, Fig. 3(b)). Apart from the elevated poleward velocities in the upper 500 m, alongshore velocity is weakly poleward throughout the upper 1000 m of the water column resolved by the OS38 (Fig. 4(e)). When comparing the baroclinic structure of the observations to the baroclinic structure of the different CTW modes, it becomes obvious that due to the missing flow reversal in our observations, the observations are best described by a first mode CTW. This mode features poleward flow throughout the upper 1500 m (Fig. 4(b)). The maximum of alongshore flow, on the other hand, is covering an area of the section better represented by a second mode CTW (Fig. 4(c)). However, it is possible that below the poleward flow of a first mode CTW, the equatorward Chile-Peru Deep Coastal Current acts to reduce poleward velocities at depth between 500 m and 800 m.

https://doi.org/10.5194/os-2019-93
Preprint. Discussion started: 5 August 2019

Similar to the velocity structure, SLA signals also support an association of the intensified poleward flow to the passage of a downwelling CTW. As discussed in the previous section, a local SLA increase was observed at the Peruvian coast while elevated poleward velocities within the PCUC depth range were present.

Bandpass-filtered SLA data from near the continental slope (section 3.3) indicates a positive SLA off Peru and Ecuador between the equator and about 14°S during this period (Fig. 5). The positive SLA along the coast propagates poleward at a velocity not inconsistent with a propagation speed of 3.1 ms^{-1}, the phase speed of the first CTW mode (Fig. 4). Moreover, when looking at SLA along the equator, there is a coherent signal starting at about 95 °W moving eastwards to the eastern boundary and arriving at about the same time when the SLA maximum of the coast is developing. Again, signal propagation from west to east is indicated, which is in agreement with the phased speed of a first vertical mode equatorial Kelvin waves (e.g. Yu and McPhaden, 1999). The SLA indicates the propagation of negative anomalies corresponding to an upwelling wave about 20 days earlier and with and origin west of 140 °W (Fig. 5) the arrival of this potential upwelling wave fits with the downward tilt in the SLA between April 25 and May 3(Fig. 2(c)) and may contribute to the weak poleward flow by causing equatorward velocity anomalies.

A downwelling CTW would cause an increase of the PCUC and SLA suggest the existence of such a wave. A first mode downwelling CTW would induce poleward transport across the upper 1500 m and we see poleward transport throughout the measurement range in the upper 1000 m. The existence of positive of a coherent high SLA along the eastern Equator and the South-American coast with poleward propagation does support the existence of a downwelling wave generated around 95 °W as well, while the speed of the propagation suggests a first mode wave.

4.3 Response of hydrographic conditions to the PCUC intensification

In the following we will analyse if the changes in circulation affect the hydrographic conditions by changing the alongshore advection.

Upwelling causes a decline of SST towards the coast (Fig. 1) and the decline of surface temperature toward the coast was seen in conservative temperature along the 12 °S section as well (Fig. 6(a) and (b)). However, the upwelling was restricted to the upper 50 m, deeper isotherms and isopycnals were bending downwards before intersecting the seafloor (Fig. 6(a) and (b)), not providing an isopycnal pathway towards the surface. The PCUC intensification co-occurred with a downward displacement of the isopycnals and isotherms (Fig. 6(b)). This caused an increase in temperature in bottom waters below 50 m depth (Fig. 6(c)), the largest warming of more than 0.5 °C occurred between 100 and 200 m depth, on the other hand surface temperatures decreased over the same time period.

Absolute salinity featured a shallow subsurface salinity maximum at about 25 m depth originating offshore and extending over the slope and shelf (Fig. 6(d) and (e)). Below this salinity maximum the isohalines were bending downward towards the bottom. During the PCUC increase the salinity in bottom waters below 100 m increased but on the upper shelf in the top 100 m it decreased (Fig. 6(f)).

https://doi.org/10.5194/os-2019-93
Preprint. Discussion started: 5 August 2019

Dissolved oxygen concentrations off Peru were characterized by a sharp oxycline above the anoxic OMZ (Fig. 6(g) and (h)). During the beginning of the measurement program from April 18 to May 3, oxygen concentrations decreased from slightly supersaturated concentrations at the surface to anoxia within the upper 100 m of the water column (Fig. 6(g)). At depth between 450 and 500 m, oxygen concentrations started to increase again to detectable values (Fig. 6(g)). When the poleward flow intensified, low oxygen waters were found deeper in the water column following the downward displacement of the isopycnals (Fig. 6(h)). During this period, oxygen concentrations of 2 µmol kg^{-1} were found at 200 m depth in the bottom water (Fig. 6(h)), which has significant consequences for benthic and pelagic biogeochemical processes in that depth range discussed below.

In the upper water column above 400m, waters denser than 1025.9 kg m^{-3} were mainly Equatorial Subsurface Water (ESSW; Fig. 7). ESSW is characterized by a linear relationship of temperature and salinity (cf. Grados et al., 2018) and originates in the equatorial current system. Lower salinity Eastern South Pacific Intermediate Water, also situated in the depth range mentioned above was only seen in the hydrographic data from two offshore stations (Fig. 7(a)). The dominance of ESSW was not affected by the increasing poleward velocities (Fig. 7(b)) and most profiles follow the same temperature and salinity relationship in both phases. In fact, during PCUC intensification, the ESSW was the sole water mass in the upper 400m within 80 km of the coast (Fig. 7(b)).

4.4 Response of biogeochemical conditions to the PCUC intensification

Nutrients are transported poleward by the PCUC and their advection thus is likely influenced by the variability of poleward velocity. In the following we describe the observed changes in nutrient concentrations and relate them to the variability in PCUC strength.

Nitrate concentrations on the shelf and upper slope increased when the poleward flow strengthened (Fig. 8(a) and (b)). The nitrate concentrations were low at the surface and increase with depth (Fig. 8 (a) and (b)). During the initial phase, offshore surface nitrate concentrations decreased to less than 10 µmol kg^{-1} and between the 20 and 25 µmol kg^{-1} isolines at 50 and 300 m depth patches of both higher and lower concentrations occur (Fig. 8(a)). Low concentrations in bottom waters on the shelf were most prominent between 75 and 100 m depth going down to 15 µmol kg^{-1} (Fig. 8(a)). After the intensification of the PCUC, nitrate concentrations between 50 and 100 m depth offshore and 250 m in bottom waters increased to above 25 µmol kg^{-1} (Fig. 8(b)). Throughout this part of the section the increase exceeded 2.5 µmol kg^{-1} (Fig. 8(c))), including areas with an increase in excess of 5 µmol kg^{-1} and even up to 10 µmol kg^{-1}. The surface layer featured a nitrate increase in excess of 5 µmol kg^{-1} as well (Fig. 8(c)).

Nitrite concentrations in the bottom water on the shelf and upper slope were reduced by the intensified PCUC (Fig. 8 (d) and (e)). The nitrite concentrations were low outside of the OMZ and their structure featured two maxima, the main one located in the centre of the OMZ around 300 m depth reaching concentrations of 5 µmol kg^{-1} and the secondary maximum in the upper part at 150 to 200 m depth. After the intensification of the PCUC the upper boundary of nitrite containing water was displaced downwards, leaving bottom waters above 250 m depth free of nitrite (Fig. 8 (e)). The depletion of nitrite in the

https://doi.org/10.5194/os-2019-93
Preprint. Discussion started: 5 August 2019


Ocean Science
Discussions
Open Access
EGU

bottom water was coupled to the downward propagation of weakly ventilated water (Fig. 6(h)). This caused a nitrite decrease exceeding 2 µmol kg^{-1} in the bottom water around 200 m depth (Fig. 8(f)).

Ammonium concentrations were generally low or undetectable. Concentrations in excess of 0.4 µmol kg^{-1} occurred only on the upper shelf and close to the surface (Fig. 8(g) and (h)), and were indicative of remineralisation of phytoplankton detritus, with rapid removal over time of the ammonium due to phytoplankton uptake and nitrification. During the flow intensification the ammonium concentrations in the surface layer were reduced to less than 0.4 µmol kg^{-1} (Fig. 8(h)). The patchiness of ammonium concentrations caused high positive and negative differences very close to each other on the shelf (Fig. 8(i)). In the surface layer above 50 to 80 m in offshore waters, a decline of ammonium concentrations was observed.

Phosphate concentrations did not change strongly by the increased strength of the PCUC (Fig. 8(j) and (k)). Concentrations were low at the surface and increased to 2 µmol kg^{-1} at 50 m depth. Within the upper OMZ the concentrations were higher offshore than onshore (Fig. 8(j) and (k)). When the PCUC intensified, concentrations decreased below 50 m depth and above 100 m at 80 km offshore and 300 m inshore (Fig. 8(l)). A phosphate decrease of up to 0.3 µmol kg^{-1} occurred in bottom waters on the shelf at water depths shallower than 100 m.

The nitrogen deficit was reduced in the later phase of the strong PCUC (Fig. 8(m) and (n)). During the weak PCUC phase the offshore maximum deficit was located between 150 and 200 m depth exceeding 12.5 µmol kg^{-1} and the absolute maximum was a localized peak exceeding 15 µmol kg^{-1} in bottom waters just above 100 m depth (Fig. 8(m)). This maximum on the shelf was caused by low nitrate (Fig. 8(a)) and high phosphate concentrations (Fig. 8(j)), while nitrite (Fig. 8(d)) and ammonium (Fig. 8(g)) were enhanced as well. After the PCUC intensification the deficit reached 5 µmol kg^{-1} at about 70 m depth offshore and at larger depths towards the coast, intersecting the seafloor at 200 m depth (Fig. 8(n)). At greater depths the maximum deficit exceeding 12.5 µmol kg^{-1} was located offshore around 150 m depth, extending towards the coast along isopycnal surfaces. After the PCUC intensification, the nitrogen deficit in the upper 200 m inshore of 70 km was reduced (Fig. 8(o)). The maximum decrease of the deficit occurred in the bottom water just above 100 m depth exceeding 10 µmol kg^{-1}; here the maximum described above in Figure 7(m) disappeared with the PCUC intensification. Further offshore around 100 m depth the decrease of the deficits exceeded 5 µmol kg^{-1} in several patches as well (Fig. 8(o)).

The decrease in nitrogen deficit between 50 m depth and about 200 m depth (deeper toward the coast, and shallow offshore) exceeding 5 µmol kg^{-1} in its maximum agreed with the location of largest poleward flow (Fig. 3(b)). At this vertical and horizontal range nitrate was increasing by more than 2.5 µmol kg^{-1} (Fig. 8(c) and phosphate decreased (Fig. 8(l)), both changes contributed to the reduced nitrogen deficit. Nitrite concentrations decreased as well (Fig. 8(f)), but the total increase in nitrogen species still exceeded the phosphate decrease by more than the ratio implied in equation (1), with the nitrate change, dominating the change of nitrogen species.

The increase in nitrate concentrations and the decrease of the nitrogen deficit and phosphate concentrations are strongest in the upper 200 m where the intensified PCUC had its maximum during the same time period. These changes occurred when comparing both regimes in density space as well (not shown) and a nitrate increase within the ESSW was evident This

https://doi.org/10.5194/os-2019-93
Preprint. Discussion started: 5 August 2019

suggests that poleward advection in the intensified PCUC is the main cause for the changes in biogeochemical properties while changes due to vertical displacement only play a minor role, here.

5 Summary and Discussion

Measurements from an intensive physical and biogeochemical shipboard sampling program off Peru at 12 °S are used to analyse intraseasonal variability of the eastern boundary circulation and associated changes in hydrography and nutrient distributions. The most prominent finding is an intensification of poleward velocities within the depth range occupied by the PCUC that occurred throughout the last 3 weeks of May in 2017. During this period, maximum poleward velocities in the PCUC core between 50 m and 100 m depth were above 50 cm s^{-1} and the poleward flow occupied the whole water column above 1000 m depth and extended to more than 80 km offshore. In contrary, climatological poleward velocities associated with the PCUC at 12 °S are about 0.1 ms^{-1} (Chaigneau et al., 2013). Similar values of average poleward flow have been reported from regional ocean models (e.g. Montes et al., 2010; Echevin et al., 2014) and from earlier observational data (e.g. Huyer et al., 1991; Czeschel et al., 2011).

The elevated poleward velocities at the eastern boundary were likely associated with a passing downwelling CTW. Satellite SLA data indicated a poleward propagation of a positive SLA signal from the equator to beyond 14 °S that occurred simultaneously to the intensified flow at 12 °S. The SLA signal propagated at a speed consistent with the phase speed of the first vertical mode CTW. Similarly, the vertical distribution of the poleward velocity anomaly at the boundary was consistent with the cross-shore-depth velocity structure of a first vertical mode CTW.

Previous studies have identified the first vertical mode CTWs to dominate intraseasonal variability in the eastern South Pacific based on observations (Brink, 1982; Shaffer et al., 1997) and model results (Illig et al., 2018b). However, observed intraseasonal intensification of poleward flow within the depth range of the PCUC in a previous study by Pietri et al. (2014) was attributed to a second and third vertical mode CTW. They found poleward velocities long the Peruvian continental slope increasing to 40 cm s^{-1}.

Although the observed cross-shore-depth velocity structure of the CTW generally agrees with the first vertical mode solution of a linear wave model using local stratification and topography, there is disagreement in the details of the flow structure. Certainly, as also noted by Pietri et al. (2014), we are comparing observed velocities to velocity anomalies caused by CTWs, thus the observed velocity can deviate from the wave solutions due to the superposition of mean flow in the observations. Furthermore, a recent study shows differences between the theoretical CTW solutions and observations due to wave scattering not included in the wave solutions presented here (Brunner et al., 2019, in press).

The SLA data indicate that the first vertical mode CTW along the eastern boundary that arrived at our sampling site in mid-May originated in the eastern equatorial Pacific at around 95°W. A coherent signal from this region propagated eastwards along the equator and arrived at about the same time when the equatorial SLA maximum at the coast was developing. This suggested generation site is further to the east than that of most previously reported intraseasonal waves. In a recent

https://doi.org/10.5194/os-2019-93
Preprint. Discussion started: 5 August 2019

375 comprehensive study by Rydbeck et al. (2019) wind forcing variability west of 150°W was found to be the main generation mechanism of intraseasonal equatorial Kelvin waves. ASCAT (Bentamy and Fillon, 2012) wind stress data shows a reduction of easterly winds at the equator in the region around 95 °W by about 2 m s^{-1} while the SLA anomaly is developing there. Furthermore, along shore winds speed at 12 °S off Peru reduce by 4 – 5 m s^{-1} about a week prior to the arrival of the maximum SLA (not shown). This suggests that the remotely forced downwelling CTW was reinforced by a local reduction
380 of upwelling favourable winds.

The temperature and salinity conditions on the shelf remain almost unchanged despite the strongly intensified poleward flow and are only displaced downwards, suggesting that the same water mass was advected within the boundary current regime during both observational periods. The weak warming and increase in salinity are in agreement with an advection of the slightly warmer and saltier water along the PCUC path north of 12 °S (Grados et al., 2018). The SST declines despite the
385 downwelling wave which would be expected to cause warming. A downwelling CTW in March 2017 indeed has contributed to the warm SST anomalies (Echevin et al., 2018). However, the impact of CTWs on intraseasonal SST variability off Peru is limited in general (Dewitte et al., 2011; Illig et al., 2014). Specifically in May 2017 SST reduction is in agreement with both the seasonal cycle (Graco et al., 2017) and the decline of the warm Coastal El Niño with peak SST in March (e.g. Garreaud, 2018).

390 Despite being non-conservative, the changes in oxygen concentrations are small. Only in the bottom water on the upper continental slope, higher oxygen concentrations are displaced downwards. Faster advection should cause higher oxygen concentrations, because the time is shorter, in which oxygen is consumed by respiration along the PCUC path. Espinoza-Morriberón et al. (2019) attribute some of the oxygen variability associated with El Niño-Southern Oscillation to the changes in microbial respiration because advection speed and pathways change under El Niño conditions (e.g. Montes et al., 2011;
395 Espinoza-Morriberón et al., 2017). However, Zamora et al. (2012) reported uniform oxygen concentrations for waters in the PCUC; therefore there is no oxygen change due to changes in alongshore advection, explaining the weak oxygen change in our study.

The limited impact of the CTW on oxygen may be related to high oxygen concentrations present at the study site before the wave passage. Compared to time series data of Callao (Graco et al., 2017) the concentrations were in the upper range of
400 variability observed after the 1997-98 El Niño event. The 22 µmol kg^{-1} surface was located at 50 m instead of 30 m reported for the climatological state by Espinoza-Morriberón et al. (2019). Whether the higher oxygen concentrations are caused by the coastal El Niño event, in the same way that canonical El Niños are related to enhanced oxygenation (e.g. Helly and Levin, 2004; Stramma et al., 2016; Espinoza-Morriberón et al., 2019), cannot be answered with our available observational data. Coastal time series off northern Peru show an oxygenation starting in February 2017 but only a weaker signal at 12 °S
405 (ENFEN, 2017) while hydrographic profiles collected in early to mid-April at 11 and 14 °S feature a very shallow oxycline (not shown). Therefore, it remains unclear whether the higher oxygen concentrations in late-April and May at 12 °S are a local or short-term phenomenon or indeed related to the coastal El Niño event.

https://doi.org/10.5194/os-2019-93
Preprint. Discussion started: 5 August 2019

The increase in nitrate concentrations and the reduced nitrogen deficit are likely caused by the shorter advection timescales in the intensified flow. The nitrate increase occurs within the ESSW range and waters with the same T-S properties are richer in nitrate after the PCUC increase (Fig. 7), excluding changed advection pathways as a likely cause of increased nitrate load. As the ESSW is moving southward in the PCUC, the N-loss leads to an increasing deficit of nitrogen between the equator and the analysed section (Silva et al., 2009; Zamora et al., 2012). Thus, the intensified PCUC transports waters with a lower nitrogen deficit polewards. The possibility of this mechanism is tested by calculating the advection timescales from the equatorial regime: the 12 °S section is about 1800 km alongshore distance away from the equator, the advection timescale for a velocity of 40 cm s^{-1} is 52 days, compared to 160 days for a velocity of 13 cm s^{-1}, approximately the climatological PCUC velocity (Chaigneau et al., 2013). Using an N-loss of 48 nmol N $l^{-1}d^{-1}$ (combined anammox and denitrification rates in the coastal OMZ from Kalvelage et al. (2013)), 5.2 µmol N l^{-1} can be transformed during the longer advection timescale. This may explain the reduction of the nitrogen deficit by about 5 µmol N kg^{-1}, as observed throughout much of the PCUC core.

The sediments off Peru below the OMZ release phosphate into the water column (Noffke et al., 2012; Lomnitz et al., 2016) that also contributes to the nitrogen deficit. Shorter advection timescales lead to a reduced accumulation of benthic phosphate release and in fact phosphate concentrations decrease during the strong PCUC flow. However, the parallel determination of the nitrogen species and phosphate shows that changes in nitrate dominate the nitrogen deficit.

The increase of nitrate by the downwelling CTW implies that the change of alongshore advection with the increased flow is more important for the nitrate balance than the downwelling itself. The downwelling would displace the nutricline and thus low nutrient surface water downwards, lowering nutrient concentrations, which is not observed. The decline of nitrate concentrations during El Niño events has been associated with the nutricline displacement due to downwelling CTWs on interannual timescales (Graco et al., 2017; Espinoza-Morriberón et al., 2017). However, focusing on intraseasonal timescales, Echevin et al. (2014) modelled an almost cancelling of horizontal and vertical (i.e. nutricline movement) advection and a fast mode CTW not impacting nutricline depth. In a model study in the Atlantic Ocean it was shown that the total effect of CTWs on nitrate concentrations varies regionally due to a different balance of horizontal and vertical advection (Bachèlery et al., 2016), but the horizontal advection always led to an increase in nitrate.

The changes in redox state in the water column and especially the bottom water affect the biogeochemical cycling in the sediment as well. Because microbial storage of nitrate and nitrite by microorganisms in the sediment can sustain vigorous N turnover even in the absence of bottom water nitrate and nitrite (Dale et al., 2016; Sommer et al., 2016), episodic events of nitrogen supply can be associated with continuous benthic nitrogen cycling. The absence of nitrate supply due the absence of CTWs over longer time periods favours the depletion of nitrate in the water column as observed by Sommer et al. (2016) and may lead ultimately to the development of sulfidic events (Schunck et al., 2013; Dale et al., 2017; Callbeck et al., 2018).

https://doi.org/10.5194/os-2019-93
Preprint. Discussion started: 5 August 2019

6 Conclusion

Based on intensive physical and biogeochemical sampling we describe and analyse the evolution of circulation, hydrography and biogeochemistry off Peru in early 2017. Poleward velocities within the PCUC intensified far beyond the reported climatological mean in May. The propagation velocity of positive SLA along the equator and coastline suggest that the intensified current is caused by a poleward propagating downwelling CTW of the first baroclinic mode excited at about 95 °W on the equator. The transition of the circulation from a weak poleward flow to strong poleward flow decreased the timescale of alongshore advection of water from the equatorial current regime to the study site at 12°S.

The downwelling CTW is not associated with strong vertical displacements of waters; instead the advection caused by the intensified PCUC is more important. The reduction of the advection timescale does not affect conservative properties; therefore temperature and salinity changes are small. But concentrations of nutrients are affected by the reduction of time available for reduction or accumulation. This causes an increase of bioavailable nitrogen as less is lost in the OMZ by N-loss processes. The nitrogen biogeochemistry is strongly changed by the altered ratio of nitrogen to phosphorus caused by the advection due to the CTW.

On intraseasonal timescales, our study suggests an increase in nitrate due to the CTW which is opposite to the decrease observed previously on interannual timescales by CTWs (Graco et al., 2017). This shows that the impact of CTWs on nutrient biogeochemistry is a complex balance between different factors, with potentially different outcome on different timescales. Analysing the processes associated with individual intraseasonal waves is also necessary to understand the interannual effect of CTWs, which is based on varying occurrence of such waves in different years.

The high variability of circulation, nutrients and the nitrogen deficit during our observations shows the need for temporally resolved sampling as an individual section recorded may be very different to the situation only weeks later. Studying intraseasonal variability like CTWs and their impact is – other than in modelling studies (e.g. Echevin et al., 2014) – only possible by high temporally resolved sampling as done in our study or in the study by Pietri et al. (2014), which is limited to the circulation only, to be able to track the changes occurring within a few days.

Data availability

Ship based observations are available at PANGAEA (https://doi.pangaea.de/10.1594/PANGAEA.903828). Global Ocean Gridded L4 sea surface heights are made available by E.U. Copernicus Marine Service (CMEMS).

Author contributions

JL carried out the data analysis and wrote the main manuscript. JL conceived the study with MD and with input by DC, ST and MV. MD and SS lead the observational program at sea. GK calibrated and processed the CTD. AD and SS provided the

nutrient data. EA provided the ammonium data. All co-authors reviewed the manuscript and contributed to the scientific interpretation and discussion.

Competing Interests

The authors declare that they have no conflict of interest.

Acknowledgements

This study was funded by the Deutsche Forschungsgemeinschaft as part of the Sonderforschungsbereich 754 "Climate–Biogeochemistry Interactions in the Tropical Ocean". We thank the Peruvian authorities for the permission to carry out scientific work in their national waters. We thank the captains and the crew of R/V Meteor for their support during the cruises. We thank Regina Surberg and Bettina Domeyer for the nutrient analysis, all other people involved in the measurement program and Rena Czeschel for post-cruise processing of the vmADCP data. Many figures in this study use colour maps from the cmocean package (Thyng et al., 2016). Global Ocean Gridded L4 sea surface heights were made available by E.U. Copernicus Marine Service (CMEMS).

References

Albert, A., Echevin, V., Lévy, M., and Aumont, O.: Impact of nearshore wind stress curl on coastal circulation and primary productivity in the Peru upwelling system, J. Geophys. Res. Oceans, 115. doi:10.1029/2010JC006569, 2010.

Bachèlery, M.-L., Illig, S., and Dadou, I.: Forcings of nutrient, oxygen, and primary production interannual variability in the southeast Atlantic Ocean, Geophys. Res. Lett., 43, 8617-8625. doi:10.1002/2016gl070288, 2016.

Bakun, A. and Nelson, C. S.: The Seasonal Cycle of Wind-Stress Curl in Subtropical Eastern Boundary Current Regions, J. Phys. Oceanogr., 21, 1815-1834. doi:10.1175/1520-0485(1991)021<1815:TSCOWS>2.0.CO;2, 1991.

Belmadani, A., Echevin, V., Dewitte, B., and Colas, F.: Equatorially forced intraseasonal propagations along the Peru-Chile coast and their relation with the nearshore eddy activity in 1992–2000: A modeling study, J. Geophys. Res. Oceans, 117. doi:10.1029/2011JC007848, 2012.

Bentamy, A. and Fillon, D. C.: Gridded surface wind fields from Metop/ASCAT measurements, Int. J. Remote Sens., 33, 1729-1754. doi:10.1080/01431161.2011.600348, 2012.

Brandt, P., Bange, H. W., Banyte, D., Dengler, M., Didwischus, S.-H., Fischer, T., Greatbatch, R. J., Hahn, J., Kanzow, T., Karstensen, J., Körtzinger, A., Krahmann, G., Schmidtko, S., Stramma, L., Tanhua, T., and Visbeck, M.: On the role of circulation and mixing in the ventilation of oxygen minimum zones with a focus on the eastern tropical North Atlantic, Biogeosciences, 12, 489-512. doi:10.5194/bg-12-489-2015, 2015.

Brink, K. H.: A Comparison of Long Coastal Trapped Wave Theory with Observations off Peru, J. Phys. Oceanogr., 12, 897-913. doi:10.1175/1520-0485(1982)012<0897:ACOLCT>2.0.CO;2, 1982.

Brink, K. H.: Energy Conservation in Coastal-Trapped Wave Calculations, J. Phys. Oceanogr., 19, 1011-1016. doi:10.1175/1520-0485(1989)019<1011:ECICTW>2.0.CO;2, 1989.

Brink, K. H.: Stable coastal-trapped waves with stratification, topography and mean flow, MBLWHOI Library. doi:10.1575/1912/10527, 2018.

Brink, K. H. and Chapman, D. C.: Programs for computing properties of coastal-trapped waves and wind-driven motions over the continental shelf and slope, WHOI Technical Reports, Woods Hole Oceanographic Institution. doi:10.1575/1912/5368, 1987.

Brink, K. H., Halpern, D., Huyer, A., and Smith, R. L.: The physical environment of the Peruvian upwelling system, Prog. Oceanogr., 12, 285-305. doi:10.1016/0079-6611(83)90011-3, 1983.

Brunner, K., Rivas, D. and Lwiza, K. M. M.: Application of classical coastal trapped wave theory to high scattering regions, J. Phys. Oceanogr., doi:10.1175/JPO-D-18-0112.1, 2019, in press.

Callbeck, C. M., Lavik, G., Ferdelman, T. G., Fuchs, B., Gruber-Vodicka, H. R., Hach, P. F., Littmann, S., Schoffelen, N. J., Kalvelage, T., Thomsen, S., Schunck, H., Löscher, C. R., Schmitz, R. A., and Kuypers, M. M. M.: Oxygen minimum zone cryptic sulfur cycling sustained by offshore transport of key sulfur oxidizing bacteria, Nat. Commun., 9. doi:10.1038/s41467-018-04041-x, 2018.

Carr, M.-E.: Estimation of potential productivity in Eastern Boundary Currents using remote sensing, Deep Sea Res. Part II, 49, 59-80. doi:10.1016/S0967-0645(01)00094-7, 2002.

Chaigneau, A., Dominguez, N., Eldin, G., Vasquez, L., Flores, R., Grados, C., and Echevin, V.: Near-coastal circulation in the Northern Humboldt Current System from shipboard ADCP data, J. Geophys. Res. Oceans, 118, 5251-5266. doi:10.1002/jgrc.20328, 2013.

Chang, B. X., Devol, A. H., and Emerson, S. R.: Denitrification and the nitrogen gas excess in the eastern tropical South Pacific oxygen deficient zone, Deep Sea Res. Part I, 57, 1092-1101. doi:10.1016/j.dsr.2010.05.009, 2010.

Chavez, F. P., Bertrand, A., Guevara-Carrasco, R., Soler, P., and Csirke, J.: The northern Humboldt Current System: Brief history, present status and a view towards the future, Prog. Oceanogr., 79, 95-105. doi:10.1016/j.pocean.2008.10.012, 2008.

Codispoti, L. A.: An oceanic fixed nitrogen sink exceeding 400 Tg N a^{-1} vs the concept of homeostasis in the fixed-nitrogen inventory, Biogeosciences, 4, 233-253. doi:10.5194/bg-4-233-2007, 2007.

Czeschel, R., Stramma, L., Schwarzkopf, F. U., Giese, B. S., Funk, A., and Karstensen, J.: Middepth circulation of the eastern tropical South Pacific and its link to the oxygen minimum zone, J. Geophys. Res. Oceans, 116. doi:10.1029/2010JC006565, 2011.

Dale, A. W., Graco, M., and Wallmann, K.: Strong and Dynamic Benthic-Pelagic Coupling and Feedbacks in a Coastal Upwelling System (Peruvian Shelf), Front. Mar. Sci. 4:29, doi.org/10.3389/fmars.2017.00029, 2017.

https://doi.org/10.5194/os-2019-93
Preprint. Discussion started: 5 August 2019

Dale, A. W., Sommer, S., Lomnitz, U., Bourbonnais, A., and Wallmann, K.: Biological nitrate transport in sediments on the Peruvian margin mitigates benthic sulfide emissions and drives pelagic N loss during stagnation events, Deep Sea Res. Part I, 112, 123-136. doi:10.1016/j.dsr.2016.02.013, 2016.

DeVries, T., Deutsch, C., Rafter, P. A., and Primeau, F.: Marine denitrification rates determined from a global 3-D inverse model, Biogeosciences, 10, 2481-2496. doi:10.5194/bg-10-2481-2013, 2013.

Dewitte, B., Illig, S., Renault, L., Goubanova, K., Takahashi, K., Gushchina, D., Mosquera, K. and Purca, S.: Modes of covariability between sea surface temperature and wind stress intraseasonal anomalies along the coast of Peru from satellite observations (2000–2008), J. Geophys. Res. Oceans, 116(C4), doi:10.1029/2010JC006495, 2011.

Echevin, V., Albert, A., Lévy, M., Graco, M., Aumont, O., Piétri, A., and Garric, G.: Intraseasonal variability of nearshore productivity in the Northern Humboldt Current System: The role of coastal trapped waves, Cont. Shelf Res., 73, 14-30. doi:10.1016/j.csr.2013.11.015, 2014.

Echevin, V., Colas, F., Espinoza-Morriberon, D., Vasquez, L., Anculle, T., and Gutierrez, D.: Forcings and Evolution of the 2017 Coastal El Niño Off Northern Peru and Ecuador, Front. Mar. Sci., 5, 367. doi:10.3389/fmars.2018.00367, 2018.

ENFEN: Technical Report ENFEN no 3 2017, Comité Multisectorial encargado del Estudio Nacional del Fenómeno El Niño (Enfen). [online] Available from: https://www.dhn.mil.pe/Archivos/oceanografia/enfen/informe-tecnico/03-2017.pdf, 2017.

Enfield, D. B., Cornejo-Rodriguez, M. D., Smith, R. L., and Newberger, P. A.: The equatorial source of propagating variability along the Peru coast during the 1982–1983 El Niño, J. Geophys. Res. Oceans, 92, 14335-14346. doi:10.1029/JC092iC13p14335, 1987.

Espinoza-Morriberón, D., Echevin, V., Colas, F., Tam, J., Gutierrez, D., Graco, M., Ledesma, J. and Quispe-Ccalluari, C.: Oxygen Variability During ENSO in the Tropical South Eastern Pacific, Front. Mar. Sci., 5, 526, doi:10.3389/fmars.2018.00526, 2019.

Espinoza-Morriberón, D., Echevin, V., Colas, F., Tam, J., Ledesma, J., Vásquez, L., and Graco, M.: Impacts of El Niño events on the Peruvian upwelling system productivity, J. Geophys. Res. Oceans. doi:10.1002/2016JC012439, 2017.

Fischer, J., Brandt, P., Dengler, M., Müller, M., and Symonds, D.: Surveying the Upper Ocean with the Ocean Surveyor: A New Phased Array Doppler Current Profiler, J. Atmos. Oceanic Technol., 20, 742-751. doi:10.1175/1520-0426(2003)20<742:STUOWT>2.0.CO;2, 2003.

Garreaud, R. D.: A plausible atmospheric trigger for the 2017 coastal El Niño, Int. J. Climatol., 38, e1296-e1302. doi:10.1002/joc.5426, 2018.

Graco, M. I., Purca, S., Dewitte, B., Castro, C. G., Morón, O., Ledesma, J., Flores, G. and Gutiérrez, D.: The OMZ and nutrient features as a signature of interannual and low-frequency variability in the Peruvian upwelling system, Biogeosciences, 14(20), 4601–4617, doi:10.5194/bg-14-4601-2017, 2017.

Grados, C., Chaigneau, A., Echevin, V., and Dominguez, N.: Upper ocean hydrology of the Northern Humboldt Current System at seasonal, interannual and interdecadal scales, Prog. Oceanogr., 165, 123-144. doi:10.1016/j.pocean.2018.05.005, 2018.

https://doi.org/10.5194/os-2019-93
Preprint. Discussion started: 5 August 2019

Grasshoff, K., Kremling, K. and Ehrhardt, M.: Methods of seawater analysis, John Wiley & Sons., 1983.

Gruber, N.: The Dynamics of the Marine Nitrogen Cycle and its Influence on Atmospheric CO2 Variations, in The Ocean Carbon Cycle and Climate, edited by M. Follows and T. Oguz, pp. 97–148, Springer Netherlands, Dordrecht., 2004.

Gruber, N. and Sarmiento, J. L.: Global patterns of marine nitrogen fixation and denitrification, Global Biogeochem. Cycles, 11, 235-266. doi:10.1029/97GB00077, 1997

Gunther, E. R.: A report on oceanographical investigations in the Peru Coastal Current, Discovery Rep., 13, 107–276, 1936.

Gutiérrez, D., Enríquez, E., Purca, S., Quipúzcoa, L., Marquina, R., Flores, G. and Graco, M.: Oxygenation episodes on the continental shelf of central Peru: Remote forcing and benthic ecosystem response, Prog. Oceanogr., 79(2–4), 177–189, doi:10.1016/j.pocean.2008.10.025, 2008.

Helly, J. J. and Levin, L. A.: Global distribution of naturally occurring marine hypoxia on continental margins, Deep Sea Res. Part I, 51, 1159-1168. doi:10.1016/j.dsr.2004.03.009, 2004.

Hill, A. E., Hickey, B. M., Shillington, F. A., Strub, P. T., Brink, K. H., Barton, E. D. and Thomas, A. C.: Eastern Ocean Boundaries, in The Seas: The Global Coastal Ocean, vol. 11, edited by A. R. Robinson and K. H. Brink, pp. 29–68, John Wiley, New York., 1998.

Holmes, R. M., Aminot, A., Kérouel, R., Hooker, B. A., and Peterson, B. J.: A simple and precise method for measuring ammonium in marine and freshwater ecosystems, Can. J. Fish. Aquat.Sci., 56, 1801-1808. doi:10.1139/f99-128, 1999.

Hormazabal, S., Shaffer, G., and Pizarro, O.: Tropical Pacific control of intraseasonal oscillations off Chile by way of oceanic and atmospheric pathways, Geophys. Res. Lett., 29. doi:10.1029/2001GL013481, 2002.

Huyer, A., Knoll, M., Paluszkiewicz, T., and Smith, R. L.: The Peru Undercurrent: a study in variability, Deep-Sea Res., 38, Supplement 1, S247 - S271. doi:10.1016/S0198-0149(12)80012-4, 1991.

Illig, S., Bachèlery, M.-L., and Cadier, E.: Subseasonal Coastal-Trapped Wave Propagations in the Southeastern Pacific and Atlantic Oceans: 2. Wave Characteristics and Connection With the Equatorial Variability, J. Geophys. Res. Oceans, 123, 3942-3961. doi:10.1029/2017JC013540, 2018b.

Illig, S., Cadier, E., Bachèlery, M.-L., and Kersalé, M.: Subseasonal Coastal-Trapped Wave Propagations in the Southeastern Pacific and Atlantic Oceans: 1. A New Approach to Estimate Wave Amplitude, J. Geophys. Res. Oceans, 123, 3915-3941. doi:10.1029/2017JC013539, 2018a

Illig, S., Dewitte, B., Goubanova, K., Cambon, G., Boucharel, J., Monetti, F., Romero, C., Purca, S. and Flores, R.: Forcing mechanisms of intraseasonal SST variability off central Peru in 2000–2008, J. Geophys. Res. Oceans, 119(6), 3548–3573, doi:10.1002/2013JC009779, 2014.

IOC, SCOR and IAPSO: The international thermodynamic equation of seawater – 2010: Calculation and use of thermodynamic properties, edited by U. (english), Intergovernmental Oceanographic Commission., 2010.

Kalvelage, T., Lavik, G., Lam, P., Contreras, S., Arteaga, L. and L&ouml: Nitrogen cycling driven by organic matter export in the South Pacific oxygen minimum zone, Nat. Geosci., 6(3), 228–234, doi:10.1038/ngeo1739, 2013.

https://doi.org/10.5194/os-2019-93
Preprint. Discussion started: 5 August 2019

Kämpf, J. and Chapman, P.: Upwelling Systems of the World: A Scientific Journey to the Most Productive Marine Ecosystems, Springer, 2016.

Karstensen, J., Schütte, F., Pietri, A., Krahmann, G., Fiedler, B., Grundle, D., Hauss, H., Körtzinger, A., Löscher, C. R., Testor, P., Vieira, N. and Visbeck, M.: Upwelling and isolation in oxygen-depleted anticyclonic modewater eddies and implications for nitrate cycling, Biogeosciences, 14(8), 2167–2181, doi:10.5194/bg-14-2167-2017, 2017.

Karstensen, J., Stramma, L., and Visbeck, M.: Oxygen minimum zones in the eastern tropical Atlantic and Pacific oceans, Prog. Oceanogr., 77, 331-350. doi:10.1016/j.pocean.2007.05.009, 2008.

Klenz, T., Dengler, M., and Brandt, P.: Seasonal Variability of the Mauritania Current and Hydrography at 18°N, J. Geophys. Res. Oceans, 123, 8122-8137. doi:10.1029/2018jc014264, 2018.

Lomnitz, U., Sommer, S., Dale, A. W., Löscher, C. R., Noffke, A., Wallmann, K., and Hensen, C.: Benthic phosphorus cycling in the Peruvian oxygen minimum zone, Biogeosciences, 13, 1367-1386. doi:10.5194/bg-13-1367-2016, 2016.

McCreary, J. P. and Chao, S.-Y.: Three-dimensional shelf circulation along an eastern ocean boundary, J. Mar. Res., 43, 13-36. doi:10.1357/002224085788437316, 1985.

McDougall, T. J. and Barker, P. M.: Getting started with TEOS-10 and the Gibbs Seawater (GSW) oceanographic toolbox, SCOR/IAPSO WG 127, 2011.

Montes, I., Colas, F., Capet, X., and Schneider, W.: On the pathways of the equatorial subsurface currents in the eastern equatorial Pacific and their contributions to the Peru-Chile Undercurrent, J. Geophys. Res. Oceans, 115. doi:10.1029/2009JC005710, 2010.

Montes, I., Schneider, W., Colas, F., Blanke, B., and Echevin, V.: Subsurface connections in the eastern tropical Pacific during La Niña 1999–2001 and El Niño 2002–2003, J. Geophys. Res. Oceans, 116. doi:10.1029/2011JC007624, 2011.

Noffke, A., Hensen, C., Sommer, S., Scholz, F., Bohlen, L., Mosch, T., Graco, M. and Wallmann, K.: Benthic iron and phosphorus fluxes across the Peruvian oxygen minimum zone, Limnol. Oceanogr., 57(3), 851–867, doi:10.4319/lo.2012.57.3.0851, 2012.

Paulmier, A. and Ruiz-Pino, D.: Oxygen minimum zones (OMZs) in the modern ocean, Prog. Oceanogr., 80, 113-128. doi:10.1016/j.pocean.2008.08.001, 2009.

Pennington, J. T., Mahoney, K. L., Kuwahara, V. S., Kolber, D. D., Calienes, R., and Chavez, F. P.: Primary production in the eastern tropical Pacific: A review, Prog. Oceanogr., 69, 285-317. doi:10.1016/j.pocean.2006.03.012, 2006.

Penven, P., Echevin, V., Pasapera, J., Colas, F., and Tam, J.: Average circulation, seasonal cycle, and mesoscale dynamics of the Peru Current System: A modeling approach, J. Geophys. Res. Oceans, 110. doi:10.1029/2005JC002945, 2005.

Pietri, A., Echevin, V., Testor, P., Chaigneau, A., Mortier, L., Grados, C., and Albert, A.: Impact of a coastal-trapped wave on the near-coastal circulation of the Peru upwelling system from glider data, J. Geophys. Res. Oceans, 119, 2109-2120. doi:10.1002/2013JC009270, 2014.

Pizarro, O., Shaffer, G., Dewitte, B., and Ramos, M.: Dynamics of seasonal and interannual variability of the Peru-Chile Undercurrent, Geophys. Res. Lett., 29, 22-1 - 22-4. doi:10.1029/2002GL014790, 2002.

Ramos, M., Dewitte, B., Pizarro, O., and Garric, G.: Vertical propagation of extratropical Rossby waves during the 1997-1998 El Niño off the west coast of South America in a medium-resolution OGCM simulation, J. Geophys. Res., 113. doi:10.1029/2007jc004681, 2008.

Revsbech, N. P., Larsen, L. H., Gundersen, J., Dalsgaard, T., Ulloa, O., and Thamdrup, B.: Determination of ultra-low oxygen concentrations in oxygen minimum zones by the STOX sensor, Limnol. Oceanogr. Methods, 7, 371-381. doi:10.4319/lom.2009.7.371, 2009.

Rydbeck, A. V., Jensen, T. G., and Flatau, M.: Characterization of Intraseasonal Kelvin Waves in the Equatorial Pacific Ocean, J. Geophys. Res. Oceans, 124, 2028-2053. doi:10.1029/2018jc014838, 2019.

Sakamoto, C. M., Johnson, K. S., and Coletti, L. J.: Improved algorithm for the computation of nitrate concentrations in seawater using an in situ ultraviolet spectrophotometer, Limnol. Oceanogr. Methods, 7, 132-143. doi:10.4319/lom.2009.7.132, 2009.

Schunck, H., Lavik, G., Desai, D. K., Großkopf, T., Kalvelage, T., Löscher, C. R., Paulmier, A., Contreras, S., Siegel, H., Holtappels, M., Rosenstiel, P., Schilhabel, M. B., Graco, M., Schmitz, R. A., Kuypers, M. M. M. and LaRoche, J.: Giant Hydrogen Sulfide Plume in the Oxygen Minimum Zone off Peru Supports Chemolithoautotrophy, PLoS One, 8(8), 1–18, doi:10.1371/journal.pone.0068661, 2013.

Shaffer, G., Pizarro, O., Djurfeldt, L., Salinas, S., and Rutllant, J. (1997). Circulation and Low-Frequency Variability near the Chilean Coast: Remotely Forced Fluctuations during the 1991–92 El Niño, Journal of Physical Oceanography, 27, 217-235. doi:10.1175/1520-0485(1997)027<0217:CALFVN>2.0.CO;2, 1997.

Silva, N., Rojas, N., and Fedele, A.: Water masses in the Humboldt Current System: Properties, distribution, and the nitrate deficit as a chemical water mass tracer for Equatorial Subsurface Water off Chile, Deep Sea Res. Part II, 56, 1004-1020. doi:10.1016/j.dsr2.2008.12.013, 2009.

Sommer, S., Gier, J., Treude, T., Lomnitz, U., Dengler, M., Cardich, J., and Dale, A. W.: Depletion of oxygen, nitrate and nitrite in the Peruvian oxygen minimum zone cause an imbalance of benthic nitrogen fluxes, Deep Sea Res. Part I, 112, 113-122. doi:10.1016/j.dsr.2016.03.001, 2016.

Sommer, S., Dengler, M. and Shipboard Scientific Party.: Benthic element cycling, fluxes and transport of nutrients and trace metals across the benthic boundary layer in the Peruvian oxygen minimum zone (SFB 754), Cruise No. 137, 06.05. - 29.05.2017, Callao (Peru) - Callao, METEOR-Berichte, doi:10.2312/cr_m137, 2019.

Stramma, L., Fischer, T., Grundle, D. S., Krahmann, G., Bange, H. W., and Marandino, C. A.: Observed El Niño conditions in the eastern tropical Pacific in October 2015, Ocean Sci., 12, 861-873. doi:10.5194/os-12-861-2016, 2016.

Strub, P. T., Mesias, J. M., Montecino, V., Rutllant, J. and Salinas, S.: Coastal ocean circulation off western South America, in The Seas: The Global Coastal Ocean, vol. 11, edited by A. R. Robinson and K. H. Brink, pp. 273–313, John Wiley, New York., 1998.

Thomsen, S., Kanzow, T., Krahmann, G., Greatbatch, R. J., Dengler, M., and Lavik, G.: The formation of a subsurface anticyclonic eddy in the Peru-Chile Undercurrent and its impact on the near-coastal salinity, oxygen, and nutrient distributions, J. Geophys. Res. Oceans, 121, 476-501. doi:10.1002/2015JC010878, 2016.

Thomsen, S., Karstensen, J., Kiko, R., Krahmann, G., Dengler, M., and Engel, A.: Remote and local drivers of oxygen and nitrate variability in the shallow oxygen minimum zone off Mauritania in June 2014, Biogeosciences, 16, 979-998. doi:10.5194/bg-16-979-2019, 2019.

Thyng, K. M., Greene, C. A., Hetland, R. D., Zimmerle, H. M. and DiMarco, S. F.: True Colors of Oceanography: Guidelines for Effective and Accurate Colormap Selection, Oceanography, 29, doi:10.5670/oceanog.2016.66, 2016.

Winkler, L. W.: Die Bestimmung des im Wasser gelösten Sauerstoffes, Ber. Dtsch. Chem. Ges., 21(2), 2843–2854, doi:10.1002/cber.188802102122, 1888.

Yu, X., and McPhaden, M. J.: Seasonal Variability in the Equatorial Pacific, J. Phys. Oceanogr., 29, 925-947. doi:10.1175/1520-0485(1999)029<0925:SVITEP>2.0.CO;2, 1999.

Zamora, L. M., Oschlies, A., Bange, H. W., Huebert, K. B., Craig, J. D., Kock, A., and Löscher, C. R.: Nitrous oxide dynamics in low oxygen regions of the Pacific: insights from the MEMENTO database, Biogeosciences, 9, 5007-5022. doi:10.5194/bg-9-5007-2012, 2012.

https://doi.org/10.5194/os-2019-93
Preprint. Discussion started: 5 August 2019

Ocean Science
Discussions
Open Access
EGU

680 **Table 1: Dates of R/V Meteor cruises conducted within the ETSP in 2017 including sampling time and number of CTD stations collected 12°S.**

R/V Meteor cruise	Dates in 2017	Sampling duration along 12°S	CTD/nutrient stations at 12°S
M135	March 2 – April 8	2 days	
M136	April 18 – May 3	15 days	59 profiles
M137	May 6 – 29	23 days	92 profiles
M138	June 1 – July 5	1 day	

https://doi.org/10.5194/os-2019-93
Preprint. Discussion started: 5 August 2019

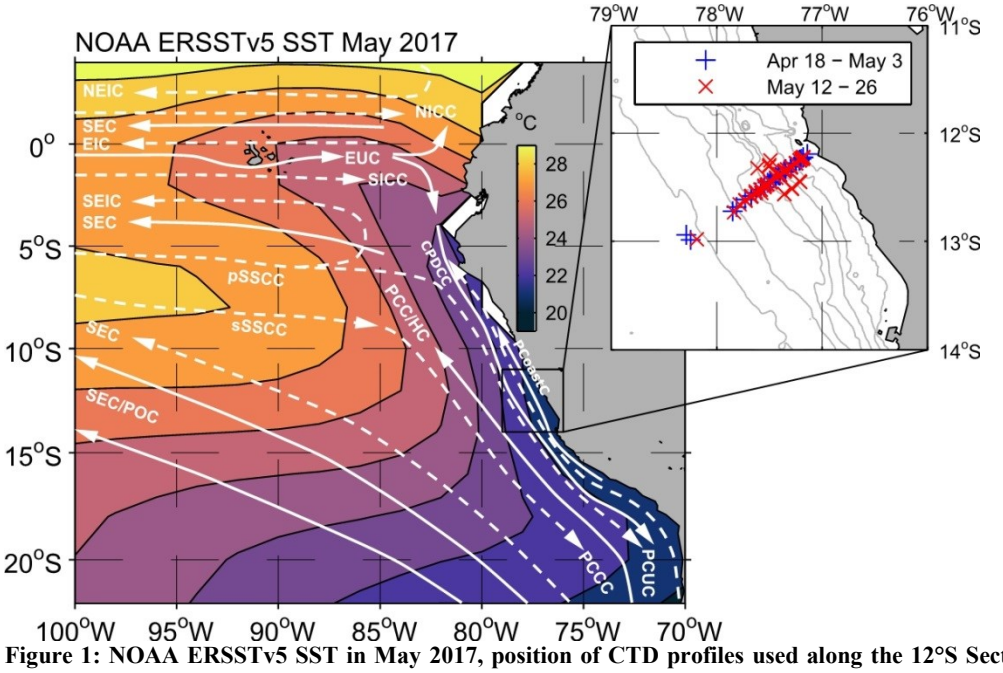

Figure 1: NOAA ERSSTv5 SST in May 2017, position of CTD profiles used along the 12°S Section in the insert. Current bands (after Brandt et al., 2015) overlaid are: for the surface layer (white solid arrows), the South Equatorial Current (SEC), the Equatorial Undercurrent (EUC), the Peru Coastal Current (PCoastC), the Peru Chile or Humboldt Current (PCC/HC), the Peru Oceanic Current (POC), and for the thermocline layer (white dashed arrows), the North Equatorial Intermediate Current (NEIC), the North Intermediate Countercurrent (NICC), the Equatorial Intermediate Current (EIC), the South Intermediate Countercurrent (SICC), the primary and secondary Southern Subsurface Countercurrents (pSSCC, sSSCC), the deeper layer of the SEC, the Chile–Peru Deep Coastal Current (CPDCC), the Peru–Chile Undercurrent (PCUC) and the Peru–Chile Countercurrent (PCCC).

https://doi.org/10.5194/os-2019-93
Preprint. Discussion started: 5 August 2019

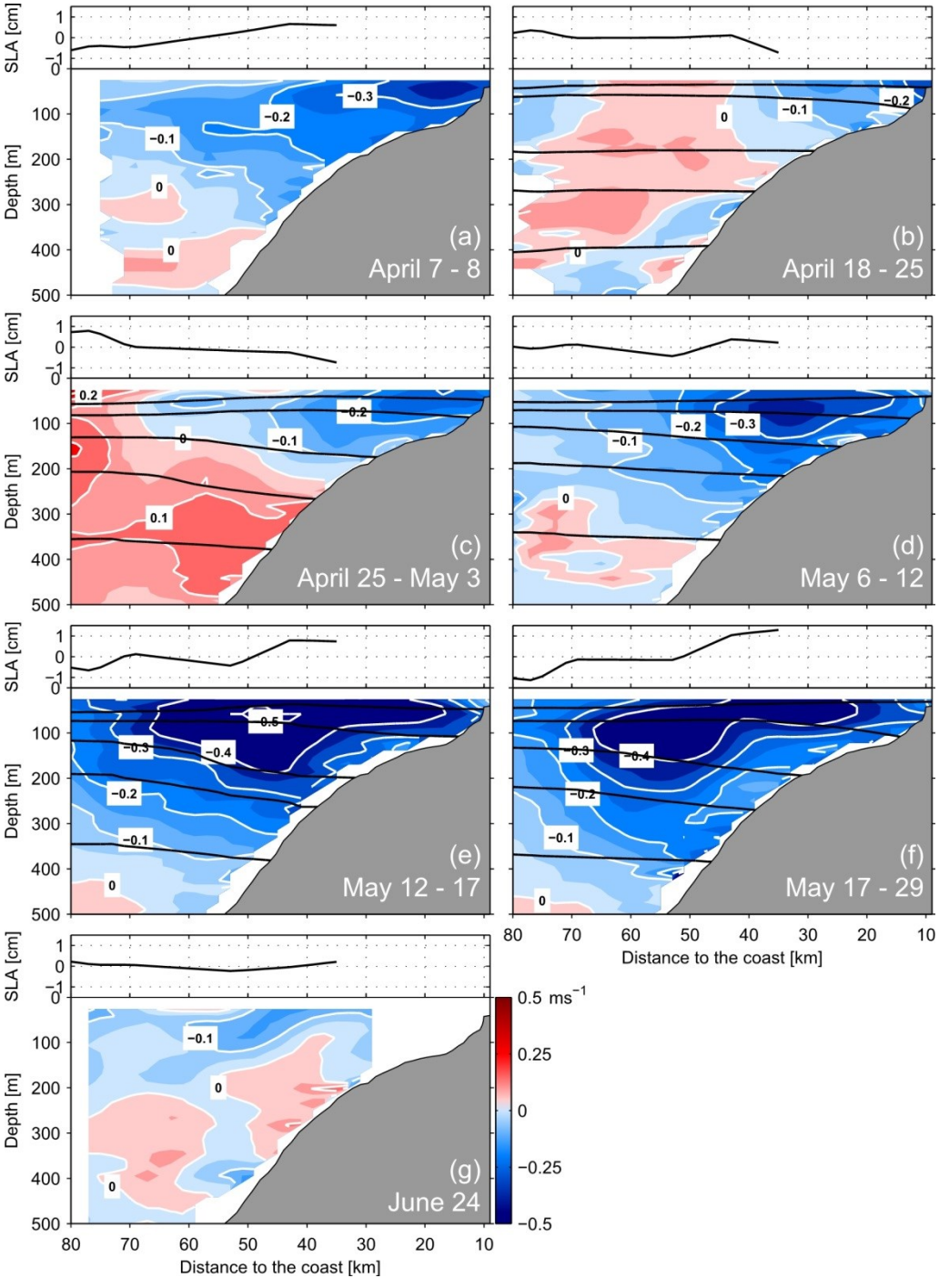

Figure 2: Alongshore circulation at the 12 °S section off Peru from OS75 vmADCP shown in colour shading, the 25.6, 25.9, 26.2, 26.4, and 26.7 kg m^{-3} isopycnals in black, the SLA is shown in the upper subpanels, during April 7 – 8 (a), April 18 – 25 (b), April 25 – May 3 (c), May 6 -12 (d), May 12 – 17 (e), May 17 – 26 (f) and June 24 (g).

https://doi.org/10.5194/os-2019-93
Preprint. Discussion started: 5 August 2019

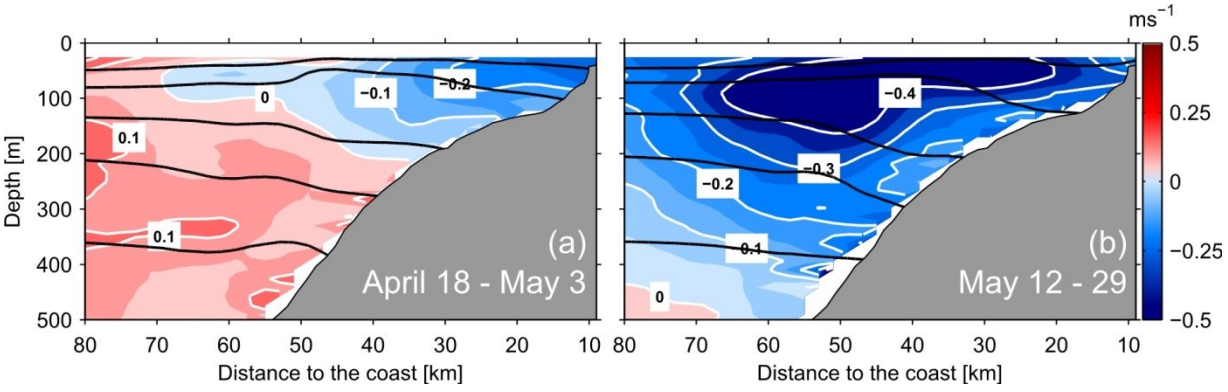

695

Figure 3: Alongshore velocity at the 12 °S section off Peru from OS75 vmADCP, the 25.6, 25.9, 26.2, 26.4, and 26.7 kg m^{-3} isopycnals in black, during April 18 – May 3, 2017 (a), May 12 – 26, 2017 (b).

https://doi.org/10.5194/os-2019-93
Preprint. Discussion started: 5 August 2019

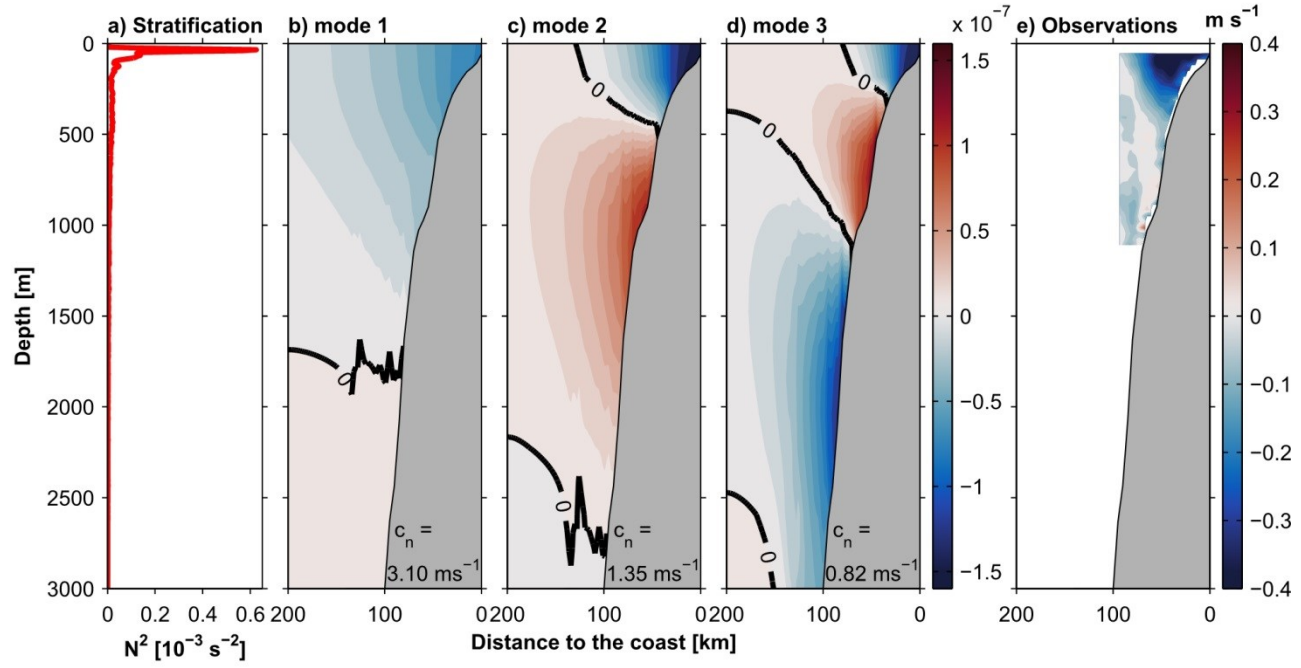

Figure 4: Alongshore velocity structure (with arbitrary amplitude) and phase speed c_n (in the lower right corner) of the first (b), second (c), and third mode (d), observed alongshore velocity from OS38 vmADCP during May 12 – 29, 2017 (e)

https://doi.org/10.5194/os-2019-93
Preprint. Discussion started: 5 August 2019

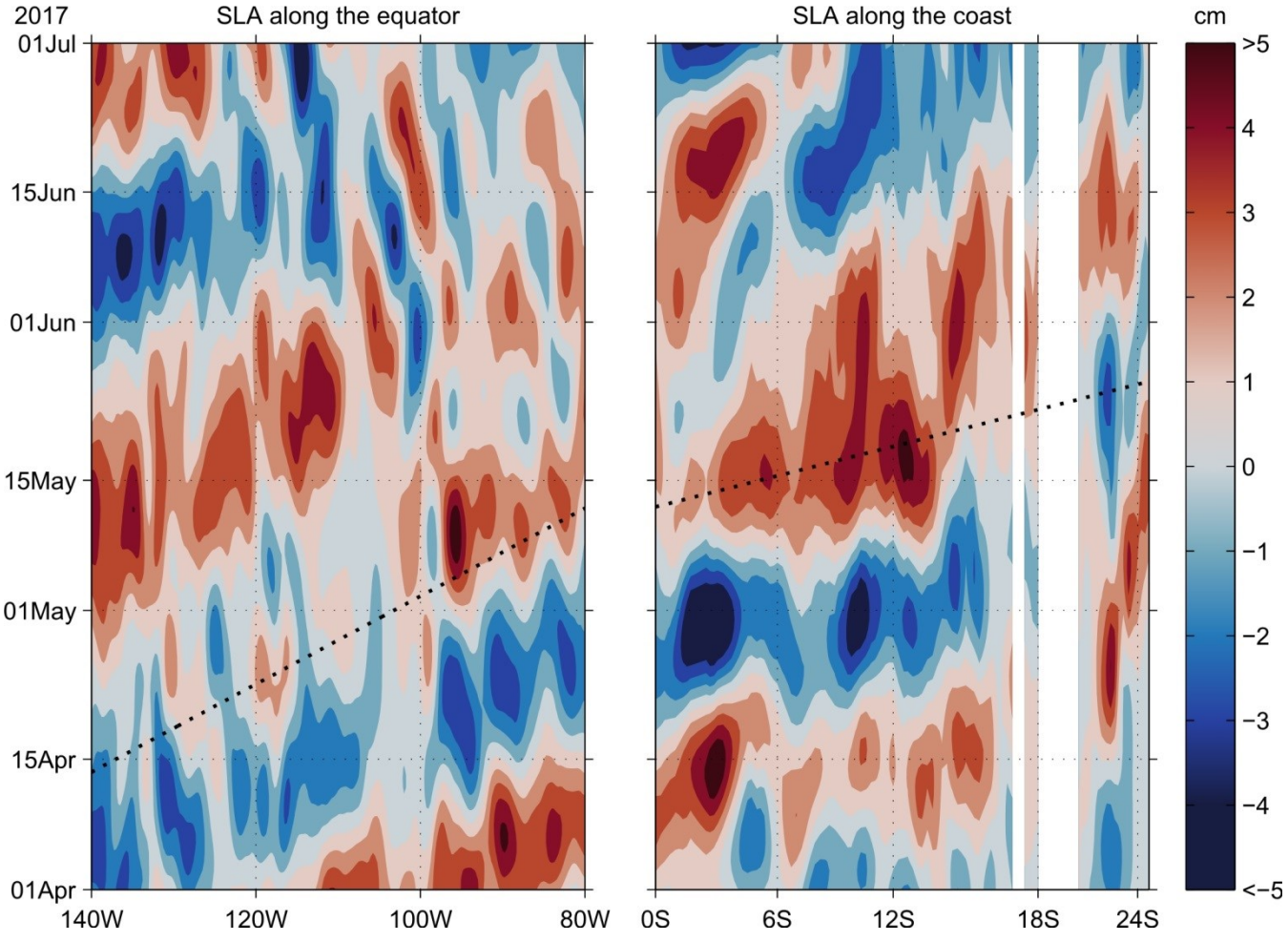

Figure 5: Bandpass filtered (20 – 90 days) sea level anomaly along the equator (left) averaged between 0.25°N and 0.25°S along the South American coast (right) averaged over the two grid point closest to the coastline, the propagation of a first mode equatorial Kelvin wave and CTW are shown as dotted black lines, phase speed of the equatorial wave is 2.72 m s^{-1} after Yu and McPhaden (1999) and 3.10 m s^{-1} for the CTW after the wave solution obtained in our study, see Figure 4.

https://doi.org/10.5194/os-2019-93
Preprint. Discussion started: 5 August 2019

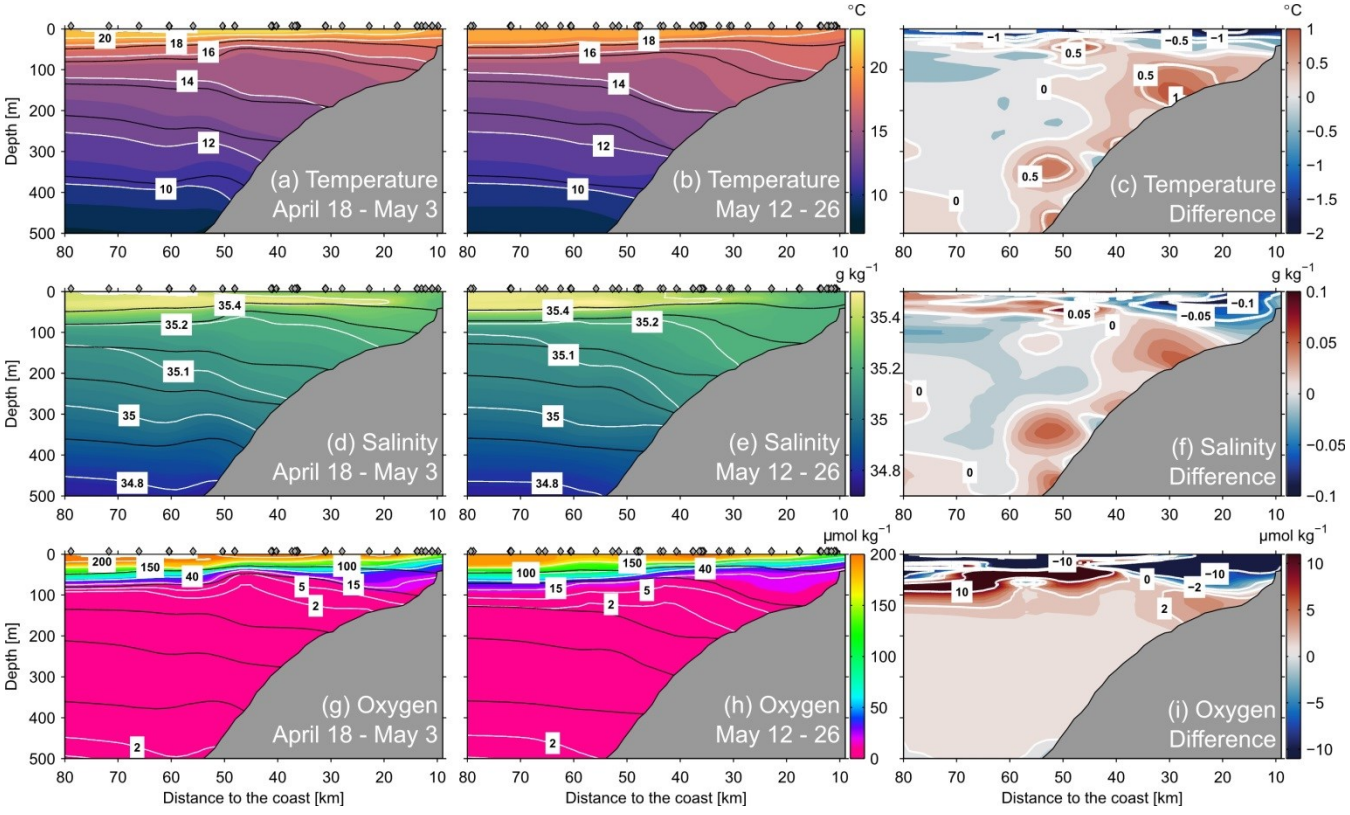

Figure 6: Conservative Temperature (upper row), absolute salinity (middle row), and oxygen (bottom row) along the 12°S section off Peru during April 18 – May 3, 2017 (left column) and May 12 – 26, 2017 (middle column), difference (right row), isolines of the shown parameter are shown in white, the 25.6, 25.9, 26.2, 26.4, and 26.7 kg m^{-3} isopycnals are shown in black, grey diamonds mark the positions of profiles.

https://doi.org/10.5194/os-2019-93
Preprint. Discussion started: 5 August 2019

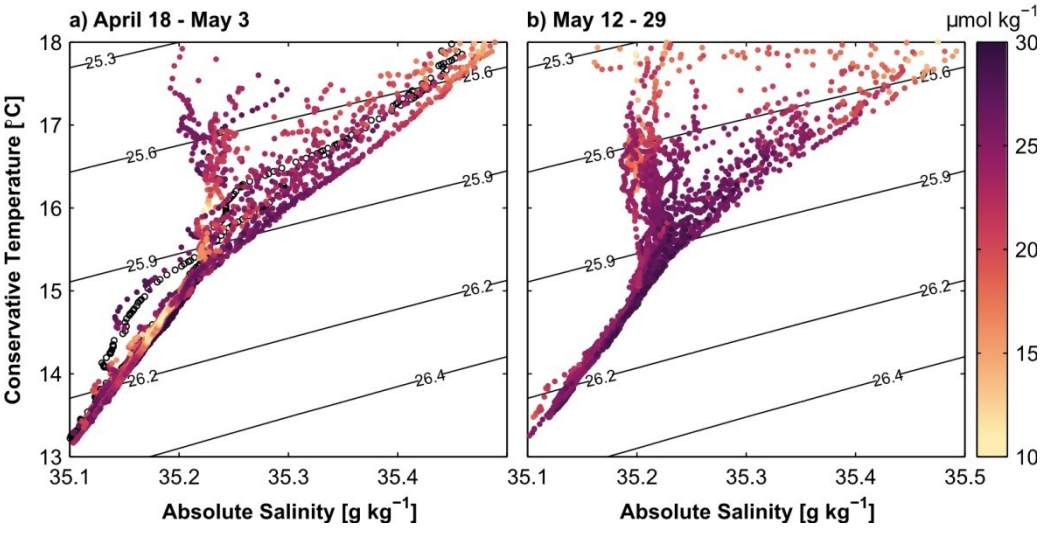

715

Figure 7: Conservative Temperature – Absolute Salinity diagram between 50 and 300m depth for CTD profiles between the 100 and 400m isobaths during April 18 – May 3, 2017 (a) and May 12 – 26, 2017 (b), contour lines show potential density anomalies corresponding to temperature and salinity on the axes, SUNA nitrate concentrations are shown as colour, empty circles are shown for profiles without SUNA data

https://doi.org/10.5194/os-2019-93
Preprint. Discussion started: 5 August 2019

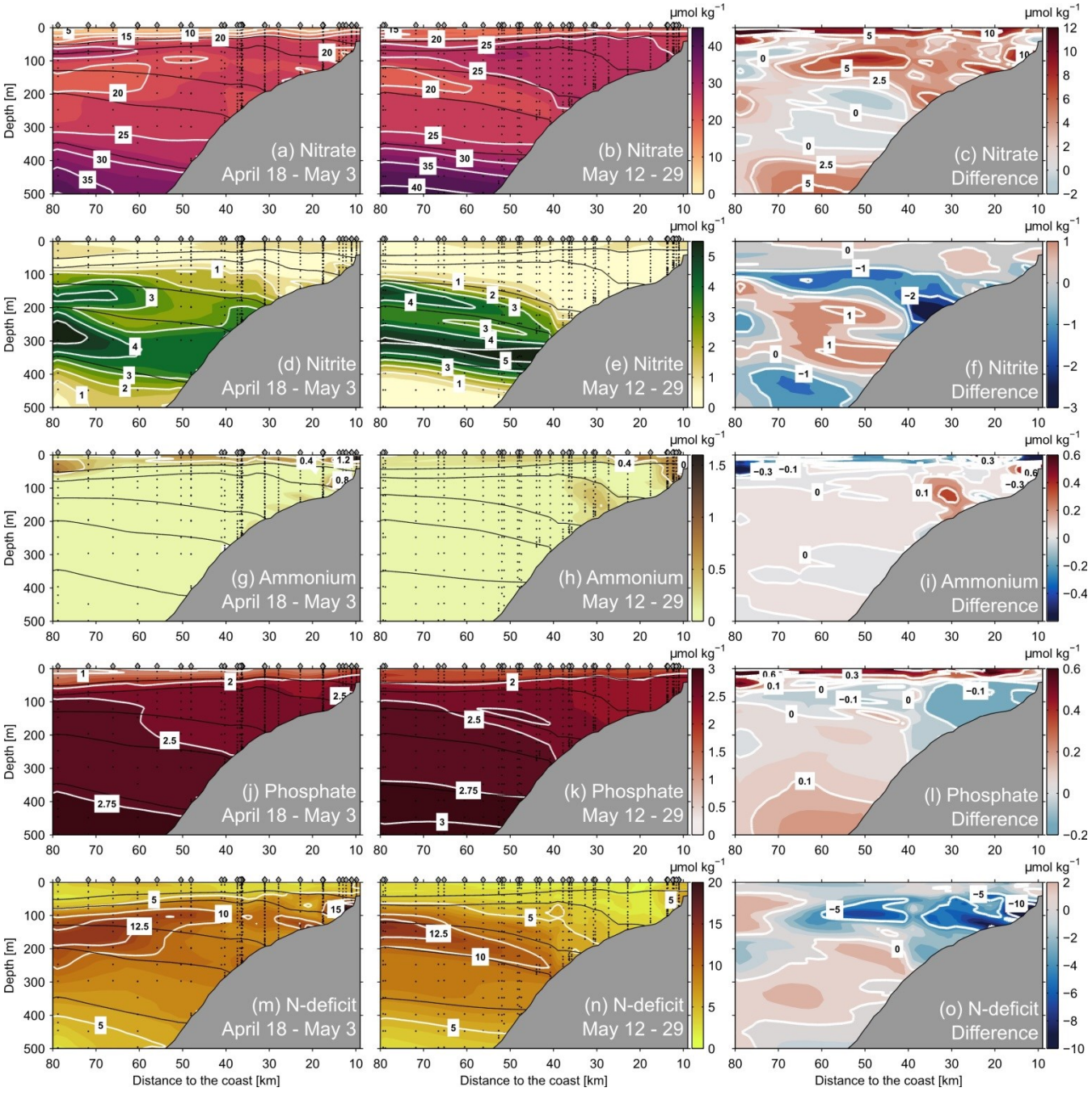

Figure 8: Nitrate (first row), nitrite (second row), ammonium (third row), phosphate (fourth row) concentrations, and nitrogen deficit (fifth row) at the 12°S section off Peru during April 18 – May 3, 2017 (left column) and May 12 – May 26, 2017 (middle column), difference (right row), isolines of the shown parameter are shown in white, the 25.6, 25.9, 26.2, 26.4, and 26.7 kg m^{-3} isopycnals are shown in black, grey diamonds mark the positions of profiles, black circles mark the position of bottle samples.